A Zeta-Based Multiport Converter with Soft-Switching and Hard-Switching Approaches for Microgrid Applications

Mojtaba Salehi
Department of Electrical and Computer Engineering
Northeastern University
Boston, MA, USA
salehi.mo@northeastern.edu

Mahshid Amirabadi
Department of Electrical and Computer Engineering
Northeastern University
Boston, MA, USA
m.amirabadi@northeastern.edu

2023 IEEE Energy Conversion Congress and Exposition (ECCE) | 979-8-3503-1644-5/23/$31.00 ©2023 IEEE | DOI: 10.1109/ECCE53617.2023.10362183

***Abstract*—This paper proposes a new Zeta-based multiport AC-link converter that serves as an interface for the interconnection of different sources and loads in multi-input/multi-output systems. The proposed converter offers improved reliability by replacing electrolytic capacitors with small film capacitors. Additionally, this converter achieves a high power density by utilizing compact high-frequency transformers instead of low-frequency transformers when isolation is needed. With only one small inductor and one small capacitor for power transfer between different sources and loads, the converter is capable of voltage step up and down over a wide range. An additional small capacitor in parallel with the inductor helps realize soft-switching in this converter. Moreover, the converter performs power conversion in a single stage, increasing the efficiency compared to multi-stage power converters. In comparison to the Ćuk-based AC-link converters, this topology uses a capacitor with a lower voltage rating. A small microgrid including a three-phase AC source, one photovoltaic source, and a three-phase AC load are considered in this paper to study and evaluate different power flow scenarios of the proposed multiport systems. The principles of the operation of the proposed topology are presented in this paper, and its performance is verified through simulations.**

Keywords—high-frequency ac link, hybrid power systems, microgrid, multiport converter, nanogrid, photovoltaics, soft-switching, zero current switching (ZCS), zero voltage switching (ZVS), Zeta converter.

I. Introduction

Over the past few decades, the attention to distributed energy (DE) systems and renewable energy sources, particularly in microgrids and nanogrids, has grown significantly. Consequently, the demand for power converters that can efficiently manage the power flow between different types of sources and loads is increasing [1].

DC-link multilevel and multiport converters are the most common configurations used in hybrid DE systems. Multilevel topologies, especially Cascaded H-bridge converters, have attracted much attention and have been widely studied recently [2-3]. However, employing These DC-link power converters may cause some reliability challenges. These challenges primarily arise from the frequent failures and the limited lifespan of some elements like electrolytic capacitors, particularly when exposed to high temperatures [4-6]. Addressing this limitation and improving overall reliability can be achieved through the elimination of electrolytic capacitors. This elimination mitigates the risk of failures and enhances the system's power density. To achieve this goal, multiport AC-link converters like Buck-Boost-based and Ćuk-based converters are introduced in [7] and [8] that offer a more reliable interaction between sources and loads. These converters extend the principles of operation employed in DC-DC converters.

A Buck-Boost-based multiport converter uses an inductor at the link to transfer power from various sources to different loads [7]. In order to minimize the size of the inductor, a high current ripple is typically allowed [9]. Additionally, the inclusion of a small capacitor in parallel with the link inductor facilitates soft switching to improve overall efficiency [10]. All the switches in this converter benefit from zero voltage turn-on and soft turn-off characteristics. Despite the advantages, the buck-boost-based multiport converter faces a high link peak current, which leads to increased conduction losses.

To address this issue, an alternative topology known as the multiport Ćuk-based converter has been introduced [8]. In this converter, a small series film capacitor at the link transfers power from different sources to different loads. Soft switching can be achieved by adding a small inductor in series with the link capacitor, providing zero current turn-off and a soft turn-on for all switches [11]. However, it is important to note that the Ćuk-based multiport converter suffers from high peak voltage across the link capacitor.

To overcome the high capacitor voltage challenge of Ćuk-based converters, a multiport Zeta-based converter, in which the link capacitor has a lower peak voltage, is proposed in this paper. The proposed converter employs a small inductor and a small capacitor to transfer the power from sources to loads. In

This material is based upon work supported by the National Science Foundation under Grant No. 2047213.

the soft-switching configuration, which is realized by adding another small capacitor in parallel with the inductor, the output side diodes benefit from zero current turn-off and zero voltage turn-on, while the input side switches benefit from zero voltage turn-on and soft turn-off. The core concept of the proposed multiport converter is introduced in [12-14]. In [12] a soft-switching Zeta inverter and a SEPIC rectifier were introduced. Hard-switching and soft-switching Zeta-based rectifiers and AC-AC converters were proposed in [13] and [14]. This paper focuses on the application of this converter in hybrid systems with a three-phase AC source, a DC source, and a three-phase AC load. The proposed topology eliminates the bulky electrolytic capacitors and makes the system more compact by using lightweight high-frequency transformers instead of line-frequency transformers in applications requiring galvanic isolation.

The article is organized as follows: Section II introduces the topology and operating principles. Subsequently, in section III, simulation results are presented to validate the performance and effectiveness of the converter. Finally, section IV provides a summary and conclusion of the paper, highlighting the key findings.

II. Operating Principles

The operating principles of the hard-switching and soft-switching Zeta-based multiport converter are discussed in parts (A) and (B) of this section, respectively.

A. Hard-switching configuration

Fig. 1 displays the isolated hard-switching Zeta-based multiport converter. In the proposed multiport configuration, a three-phase AC source and a DC source are supplying a three-phase AC load via the link capacitor (C_1 and C_2) and the input inductor (L_{in}). The inclusion of a high-frequency transformer (HFT) is optional. In non-isolated topologies, only one link capacitor is required instead of two. The link current, link voltage, and input inductor voltage waveforms during different modes are depicted in Fig. 2.

For the three-phase AC source, it is assumed that I_A^{ref}, the current reference of phase A, is positive and has the maximum absolute value among three-phase input currents. On the other hand, the current references of phases B and C (I_B^{ref} and I_C^{ref}) are negative and the absolute value of I_C^{ref} is smaller than I_B^{ref}. Similarly, in the three-phase AC load, it is assumed that V_{ABO}^{ref}, the voltage reference across phase pair AB, is positive and has the maximum absolute value among three-phase output line-to-line voltages. V_{BCO}^{ref} and V_{CAO}^{ref}, the voltage references of phase pairs BC and CA, are negative and the absolute value of V_{CAO}^{ref} is smaller than V_{BCO}^{ref}. It is also assumed that the voltage of the DC source is lower than voltages across phase pairs AB and CA in the three-phase AC source. It is obvious that based on the instantaneous values of currents and voltages, different switching states need to be selected.

In the first mode, power is transferred from the input inductor (L_{in}) to the link capacitor through the load-side antiparallel diodes, as shown in Fig. 3(a). In this mode, all switches are turned off, and the AC load diodes conduct, which results in zero unfiltered source currents and zero unfiltered load voltages. This mode continues until the link capacitor voltage increases to its maximum value (Fig. 2).

At the end of Mode 1, Q_1 and Q_5 are turned on, and this allows the input inductor to be charged with V_{AB} and initiate input mode 2 (as illustrated in Fig. 3(b)), and simultaneously, the first link capacitor discharging mode, output mode 2, begins (Fig. 3(c)). As soon as the average current of input phase B, $I_B^{average}$, equals its reference, I_B^{ref}, switch Q_5 is turned off, and switch Q_6 turns on to initiate another charging mode (input mode 3), shown in Fig. 3(d). This charging mode continues until $I_A^{average}$ meets I_A^{ref}. Once this happens, Q_1 and Q_6 are turned off, and Q_7 is turned on to charge the input inductor with the DC source voltage in input mode 4 (Fig. 3(e)).

For discharging modes, the link capacitor starts to discharge by the load phase current that has the second-highest value in output mode 2. Switches Q8, Q12, and the anti-parallel diode of Q10 conduct during this mode. When the corresponding output voltage ($V_{BCo}^{Average}$) meets its reference value, this mode ends and the last discharging mode starts.

During the last discharging mode (output mode 3), the link capacitor discharges to the load with the highest load current ($|I_{Ao}|$). In this mode, switches Q_8, Q_{12}, and Q_{13} are turned on (Fig. 3(f)). This mode continues until the link capacitor is completely discharged. It should be noted that the input inductor charging modes and the link capacitor discharging modes are controlled independently and they have different durations.

B. Soft-switching configuration

Fig. 4 shows the isolated soft-switching zeta-based multiport converter. The link current, link voltage, and the input inductor voltage waveforms for different operating modes are depicted in Fig. 5. The main difference with the hard-switching topology is that a small resonating capacitor ($C_{resonance}$) is connected in parallel with the input inductor to add the resonating modes for the soft-switching configuration.

In the first mode, all the switches are off, and the power is transferred from the input inductor (L_{in}) to the link capacitor (C_{link}) via the output side anti-parallel diodes. When the link capacitor is fully charged, and the input inductor current becomes zero, the load-side diodes turn off under zero current switching conditions (ZCS).

After this mode, the link capacitor first discharging mode and the first resonating mode start. During the first resonating mode, the voltage of the input inductor reaches V_{AB}, and the voltages across Q_1 and Q_5 become zero and they turn on under zero voltage switching (ZVS).

In input mode 3, which is the first inductor charging mode, the highest line-to-line input voltage (V_{AB}) charges the inductor (L_{in}). When the average of I_B meets I_B^{ref}, Q_5 turns off and another resonating mode starts.

In the second resonating mode, the input inductor resonates with its parallel capacitor until V_{in} reaches $|V_{AC}|$. At

this moment, Q_6 turns on under ZVS to start another inductor charging mode.

During the second inductor charging mode (input mode 5), the input inductor (L_{in}) receives power from the three-phase source with the voltage of V_{AC} until the average of I_A reaches I_A^{ref}. At this time, switches Q_1 and Q_6 are turned off and another resonating mode starts to allow V_{in} to swing to V_{DC}. Following this condition, Q_7 turns on under ZVS to charge the input inductor with V_{DC}, and the last inductor charging mode continues until the average of I_{DC} becomes equal to I_{DC}^{ref}.

By turning off Q_7, the input inductor, and its parallel capacitor resonate until the inductor voltage becomes equal to the absolute value of the link capacitor voltage. At this time, the antiparallel diodes turn on with ZVS to start the next cycle.

The link capacitor discharging modes are the same as the hard-switching case.

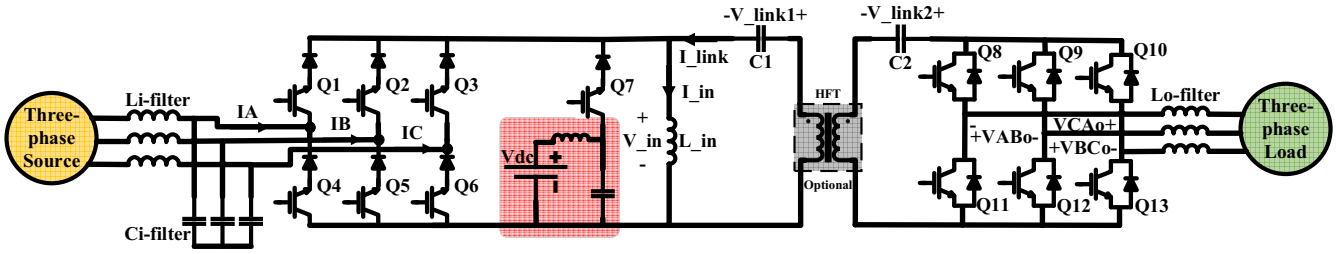

Fig. 1. Isolated hard-switching Zeta-based multiport converter.

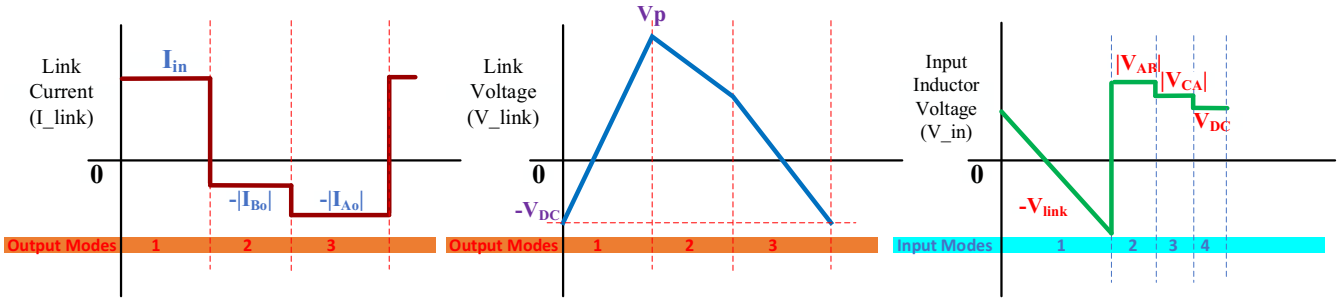

Fig. 2. Voltage and current waveforms of the link capacitor and the input inductor voltage in the hard-switching Zeta-based multiport converter.

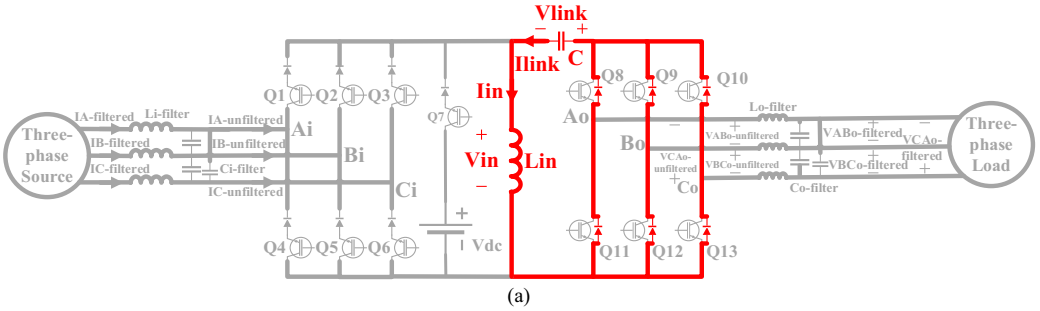

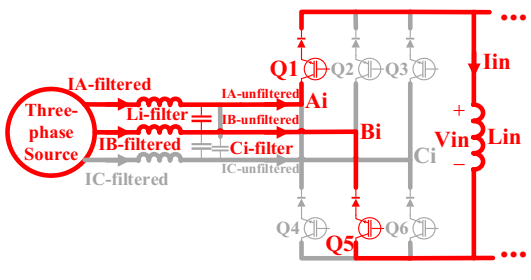

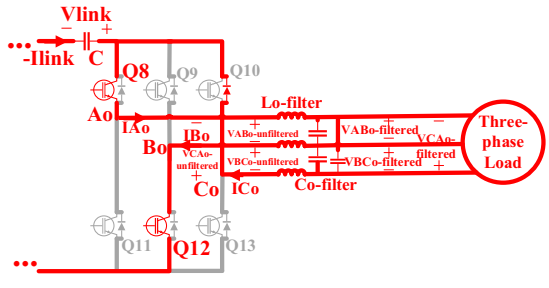

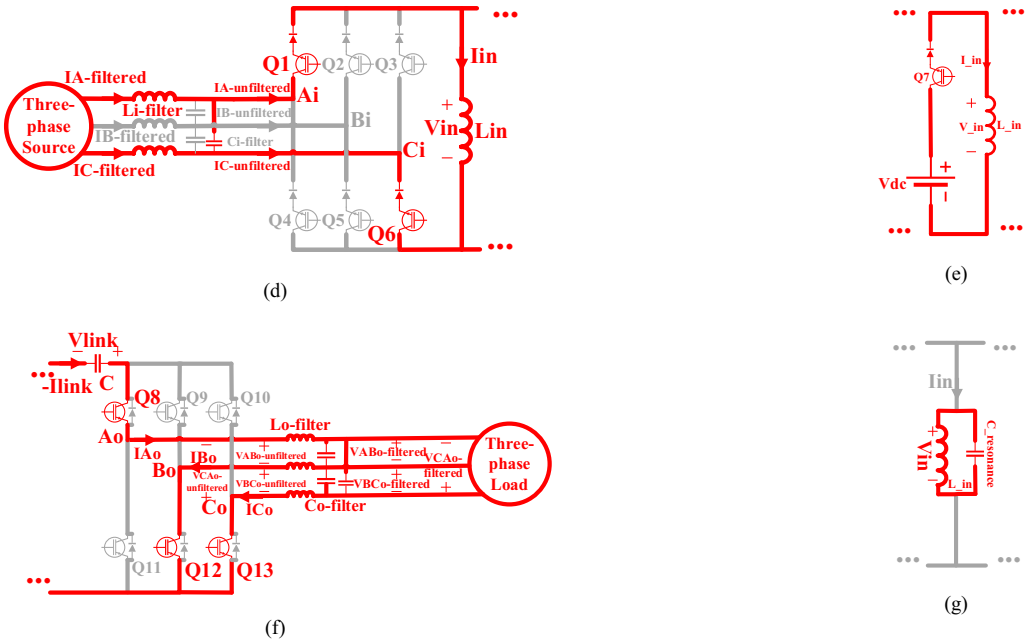

Fig. 3. (a) Behavior of the non-isolated Zeta-based multiport converter during mode 1, (b) Behavior of the non-isolated Zeta-based multiport converter during the first inductor charging mode, (c) Behavior of the non-isolated Zeta-based multiport converter during the first capacitor discharging mode, (d) Behavior of the non-isolated Zeta-based multiport converter during the second inductor charging mode, (e) Behavior of the non-isolated Zeta-based multiport converter during the third inductor charging mode, (f) Behavior of the non-isolated Zeta-based multiport converter during the second capacitor discharging mode, (g) Behavior of the non-isolated Zeta-based multiport converter during resonating modes.

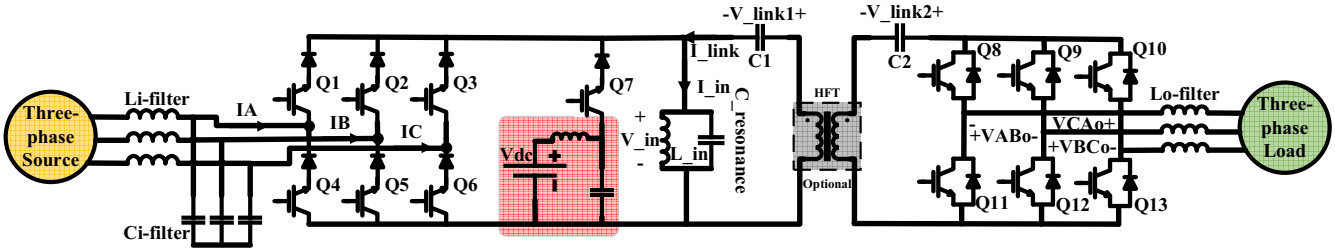

Fig. 4. Isolated soft-switching Zeta-based multiport converter.

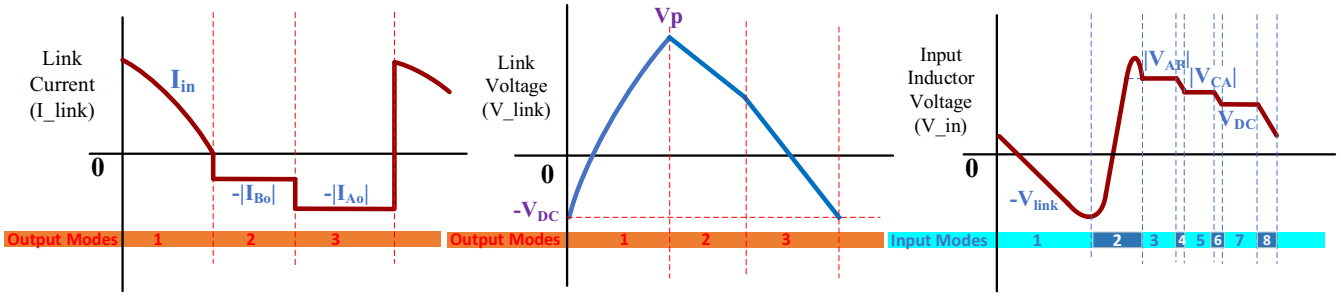

Fig. 5. Link capacitor voltage and current and the input inductor voltage in the soft-switching Zeta-based multiport converter.

III. Simulation Results

In this section, simulation results corresponding to both soft-switching and hard-switching converters are presented to verify the effectiveness of the proposed converter. The parameters of the converter are summarized in Table I.

A. Hard-switching configuration

Figures 6-9 display the simulation results corresponding to the proposed hard-switching Zeta-based multiport converter. Fig. 6 shows the voltages and currents of the link capacitor, where the link voltage is negative for a small portion of time to

allow using a capacitor with a lower voltage rating compared to the Ćuk-based converters. Fig. 7 illustrates the input inductor voltage and current waveforms. The unfiltered input currents and output voltages are depicted in Fig. 8. As mentioned in the operating principles section, the input inductor charging modes and the link capacitor discharging modes are controlled independently and they have different durations. Fig. 9 shows the filtered input currents with a THD of 2.2% and filtered output voltages with a THD of 3.5%, and the filtered input DC current.

B. Soft-switching configuration

By adding a 30 nF capacitor in parallel with the input inductor the converter can benefit from soft-switching. Simulation results corresponding to the designed soft-switching Zeta-based multiport converter are illustrated in Figs. 10- 14. The voltage and current waveforms of the link capacitor and input inductor are given in Figs. 10 and 11, respectively. Similar to the hard-switching configuration, the minimum value of the link voltage can be negative to reduce the link peak voltage compared to Ćuk-based converters. Fig. 12 presents the unfiltered input currents and output voltages during different power transferring and resonating modes. The voltage and current waveforms of the switches shown in Fig. 13 verify the soft-switching in this converter. Fig. 14 shows the filtered output three-phase voltages with a THD of 4%, filtered three-phase input currents with a THD of 1%, and the filtered input DC current.

IV. Conclusion

This paper presented a hard-switching and a soft-switching Zeta-based multiport converter that can be used in nanogrid and microgrid applications, where different types of sources and loads need to intelligently interact. Due to the elimination of the bulky electrolytic capacitors and the low-frequency transformers, the size and weight of the proposed converters are expected to be lower than traditional DC-link multiport converters. Furthermore, this topology has a lower link peak voltage compared to Ćuk-based multiport converters. In the soft-switching topology, the output side diodes benefit from zero current turn-off and zero voltage turn-on. And the input side switches benefit from zero voltage turn-on and soft turn-off.

TABLE I. Zeta-based Multiport Converter Parameters

	Link frequency	*Three-phase source and three-phase load frequency*	*Link capacitance*	*Input inductance*	*Resonance capacitance (for the soft-switching configuration)*	*Power level*	*RMS line-to-line three-phase source voltage*	*RMS line-to-line three-phase load voltage*	*DC source voltage level*
Multiport Converter	30 kHz	60 Hz	300 nF	100 µH	30 nF	50 kW	850 V	700 V	500 V

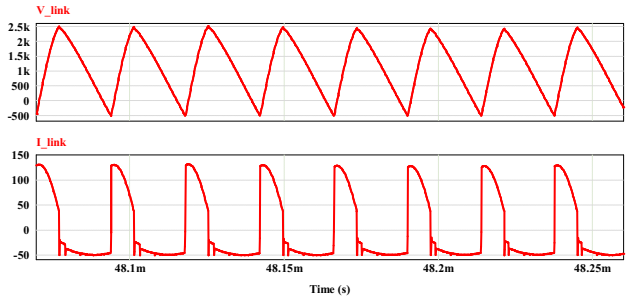

Fig. 6. Current and voltage of the link capacitor in the hard-switching Zeta-based multiport converter.

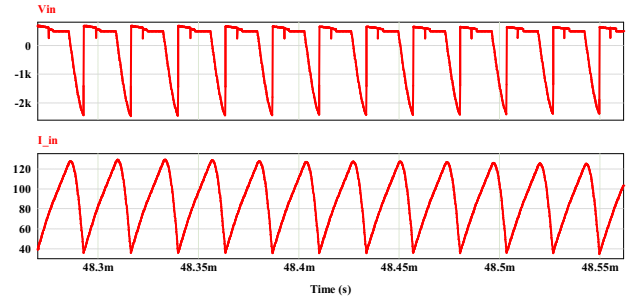

Fig. 7. Current and voltage of the input inductor in the hard-switching Zeta-based multiport converter.

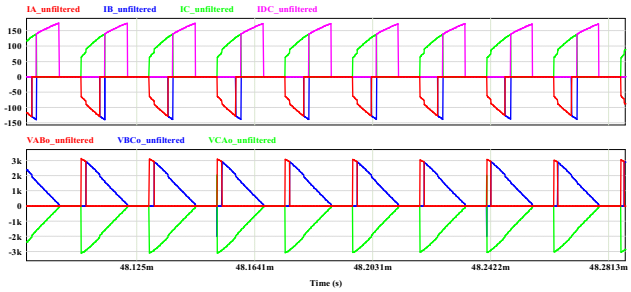

Fig. 8. Unfiltered input currents and output voltages in the hard-switching Zeta-based multiport converter.

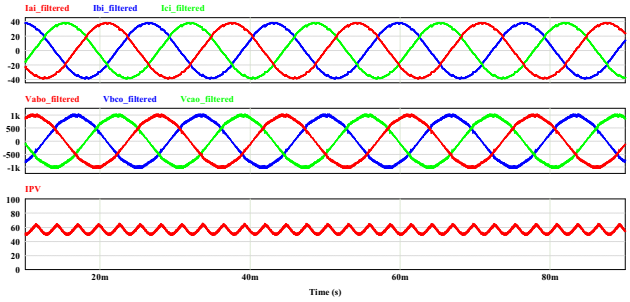

Fig. 9. Filtered ac and dc sources currents and load voltages in the hard-switching Zeta-based multiport converter.

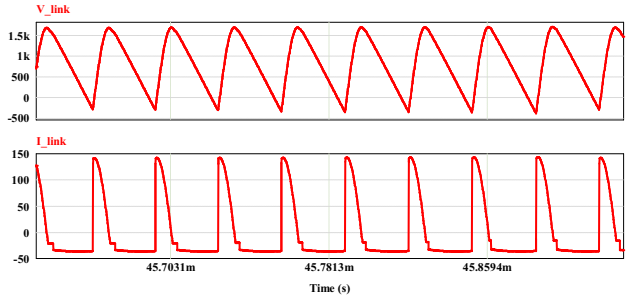

Fig. 10. Current and voltage of the link capacitor in the soft-switching Zeta-based multiport converter.

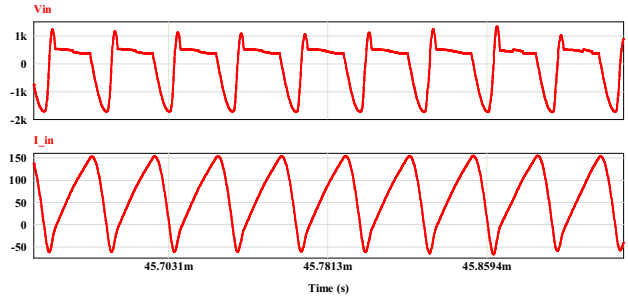

Fig. 11. Current and voltage of the input inductor in the soft-switching Zeta-based multiport converter.

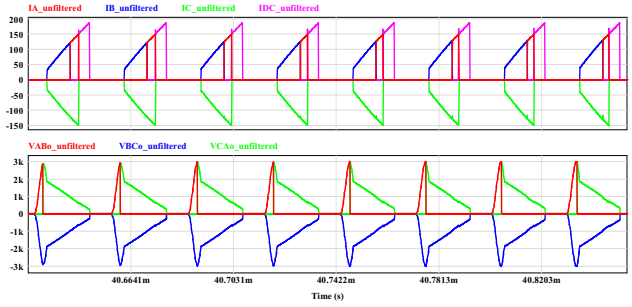

Fig. 12. Unfiltered input currents and output voltages in the soft-switching Zeta-based multiport converter.

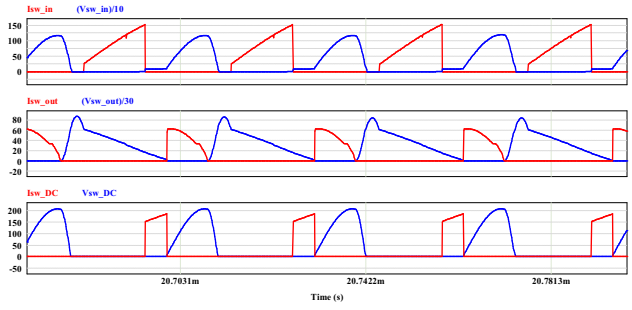

Fig. 13. Current and voltages across switches in the soft-switching Zeta-based multiport converter.

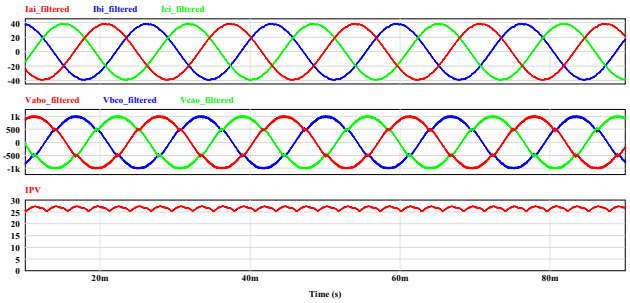

Fig. 14. Filtered source currents and load voltages in the soft-switching Zeta-based multiport converter.

ACKNOWLEDGMENT

This material is based upon work supported by the National Science Foundation under Grant No. 2047213.

REFERENCES

[1] N. Asadi, M. Hamzeh and K. Abbaskhanian, "The Impact of DSTATCOM on the Small-Signal Stability of Islanded Microgrids," 2020 11th Power Electronics, Drive Systems, and Technologies Conference (PEDSTC), Tehran, Iran, 2020, pp. 1-7, doi: 10.1109/PEDSTC49159.2020.9088455.

[2] H. Althuwaini, A. Zare and M. B. Shadmand, "An Optimal Predictive Control for Maximum Utilization of Heterogeneous Battery Energy Storage System Interfaced Cascaded Multilevel Inverters," 2022 IEEE Energy Conversion Congress and Exposition (ECCE), Detroit, MI, USA, 2022, pp. 1-7, doi: 10.1109/ECCE50734.2022.9947725.

[3] M. Salehi, M. Shahabadini, H. Iman-Eini, and M. Liserre, "Predictive Control of Grid-Connected Modified-CHB With Reserve Batteries in Photovoltaic Application Under Asymmetric Operating Condition," in IEEE Transactions on Industrial Electronics, vol. 69, no. 9, pp. 9019-9028, Sept. 2022, doi: 10.1109/TIE.2021.3113009.

[4] C.-J. Shin and J.-Y. Lee, "An electrolytic capacitor-less bi-directional EV on-board charger using harmonic modulation technique," *IEEE Trans. Power Electron.*, vol. 29, no. 10, pp. 5195 – 5203, Oct. 2013.

[5] H. Wang and F. Blaabjerg, "Reliability of capacitors for DC-link applications in power electronic converters—An overview," *IEEE Trans. Ind. Appl.*, vol. 50, no. 5, pp. 3569 – 3578, Sep./Oct. 2014.

[6] T. Friedli, J. W. Kolar, J. Rodriguez, and P. W. Wheeler, "Comparative evaluation of three-phase AC-AC matrix converter and voltage DC-link back-to-back converter systems," *IEEE Trans. Ind. Electron.*, vol. 59, no. 12, pp. 4487 – 4510, Dec. 2012.

[7] M. Amirabadi, H. A. Toliyat, and W. C. Alexander, "A Multiport AC Link PV Inverter With Reduced Size and Weight for Stand-Alone Application," IEEE Transactions on Industry Applications, vol. 49, no. 5, pp. 2217-2228, Sept.-Oct. 2013.

[8] E. Afshari and M. Amirabadi, "Single-Stage Multiport Capacitive-Link Universal Power Converter as a Solid-State Transformer for Nanogrid and Microgrid Applications," 2019 IEEE Applied Power Electronics Conference and Exposition (APEC), pp. 382-388.

[9] L. Kim and G. Cho, "New bilateral zero voltage switching AC/AC converter using high frequency partial-resonant link," in 16th Annual Conference of IEEE Industrial Electronics Society, 1990, pp. 857-862.

[10] M. Amirabadi, J. Baek, H. A. Toliyat and W. C. Alexander, "Soft-Switching AC-Link Three-Phase AC–AC Buck–Boost Converter," in IEEE Transactions on Industrial Electronics, vol. 62, no. 1, pp. 3-14, Jan. 2015, doi: 10.1109/TIE.2014.2331011.

[11] M. Khodabandeh, E. Afshari, and M. Amirabadi, "A Single-Stage Soft-Switching High-Frequency AC-Link PV Inverter: Design, Analysis, and Evaluation of Si-Based and SiC-Based Prototypes," *IEEE Transactions on Power Electronics*, vol. 34, no. 3, pp. 2312-2326, 2018.

[12] M. Khodabandeh and M. Amirabadi, "A Soft-switching Single-stage Zeta-/SEPIC-based Inverter/Rectifier," 2020 IEEE Applied Power

Electronics Conference and Exposition (APEC), New Orleans, LA, USA, 2020, pp. 3456-3463, doi: 10.1109/APEC39645.2020.9124509.

[13] M. Salehi, M. Khodabandeh and M. Amirabadi, "Zeta-Based AC-Link Universal Converter," 2022 IEEE Energy Conversion Congress and Exposition (ECCE), Detroit, MI, USA, 2022, pp. 1-7, doi: 10.1109/ECCE50734.2022.9947744.

[14] M. Salehi and M. Amirabadi, "A Soft-Switching Zeta-Based AC-Link Universal Converter," 2023 IEEE Applied Power Electronics Conference and Exposition (APEC), Orlando, FL, USA, 2023, pp. 3233-3239, doi: 10.1109/APEC43580.2023.10131175.